Effect of Filler–Elastomer Interactions on the Mechanical and Nonlinear Viscoelastic Behaviors of Chemically Modified Silica-Reinforced Solution-Polymerized Styrene Butadiene Rubber

Liangliang Qu, Guozhu Yu, Lili Wang, Chuanqing Li, Qingsong Zhao, Jing Li

Yanshan Branch of Beijing Research Institute of Chemical Industry, China Petroleum & Chemical Company (Sinopec Corp.), Beijing 102500, People's Republic of China

Received 10 October 2011; accepted 18 December 2011
DOI 10.1002/app.36677
Published online in Wiley Online Library (wileyonlinelibrary.com).

ABSTRACT: We explore the effects of surface modification of silica on mechanical and nonlinear viscoelastic behaviors of solution-polymerized styrene butadiene rubber (SSBR) filled by modified silica (M-Silica). Compared with pristine silica-filled SSBR, SSBR reinforced by M-Silica presents not only better filler dispersity and mechanical properties but also lower internal friction in the certain temperature range. The cure kinetics was investigated in term of curemeter, and the kinetics parameters of SSBR/M-Silica were found to vary from those of SSBR with pristine silica, indicating that silane coupling agent molecules grafted on the silica surface provoked an enhanced mobility of rubber chain adsorbed onto filler surface and then decreased the barrier of crosslink reaction. Analysis using tube model theory provided more evidence for the reinforcement effect of M-Silica. SSBR containing M-Silica exhibited a combination of increments in topological tube-like constraints and crosslink density in comparison with SSBR filled with pristine silica. Strain dependence of dynamic modulus revealed that the secondary network formed by silica particles was destroyed to some extent with the increase of the hydrophobic character of silica surface. Loss factor of SSBR/M-Silica was dominated by different mechanism in different temperature range, i.e., secondary filler network at glass transition temperature and rubber–filler interaction and entangled structure above room temperature. © 2012 Wiley Periodicals, Inc. J Appl Polym Sci 000: 000–000, 2012

Key words: solution styrene butadiene rubber; modified silica; silane coupling agent; nonlinear viscoelastic behaviors; mechanical properties; tube model

INTRODUCTION

Since the introduction of the so-called "Green tire" by Michelin, precipitated silica has been proved to be the filler of choice for the manufacture of high performance pneumatic passenger car tires.[1,2] Silica as a reinforcement agent provides a combination of good mechanical properties, high resilience, excellent rolling resistance, and low heat build-up.[3–5] Technological development of using silica particles instead of carbon black and some related studies of reinforcing mechanism have attracted considerable interest in both industrial and academic field.

The significant reinforcing effect exhibited by silica contrasts with the difficulty on the processability of the silica-filled rubber compounds because of the poor dispersity of silica particles in the rubber matrix. Silica particles show strong filler–filler interactions and adsorption of polar compounds in that silica is abundant in silanol groups on its surface. In order to enhance the filler dispersion, many efforts have been devoted to the surface modification of silica[6–9] and accordingly new highly dispersed silica has been developed in the recent years. One of the effective modification methods for silica is to graft the silane coupling agent (SCA) onto the silica surface via the condensation reaction between the alkoxy groups of SCA and silanol groups of silica.[10–13] To our knowledge, many published literatures have focused on the modification methods of silica and the improved properties of the rubber filled with the modified silica, but few researches paid much attention to the mechanism of reinforcement achieved by the modified silica and nonlinear viscoelastic behaviors of such filled rubber. They are usually characterized by specific nonlinear viscoelastic behaviors, including high hysteresis, stress softening (Mullins effect), and strain dependent dynamic modulus effect (Payne effect). Experimental data reported in literatures give evidence that the thermomechanical properties of filled rubbers are affected by many factors, such as molecular structure of rubbers; the

Correspondence to: L. Qu (quliangliang.bjhy@sinopec.com and echo_quliangliang@hotmail.com).

shape, size, and content of filler; and the rubber/filler interactions.[14–16] Hence, a deeper understanding of such filled rubber network is of utmost importance to explain the improved properties.

The theory of networks can be regarded as a bridge between modern condensed matter physics and applied materials science.[17,18] Most of rubber elasticity theories[19,20] usually adopt free energy to predict the stress–strain relation, but these theories are too simple to take the molecular forces and entanglement into account. Among several versions of the entanglement model of equilibrium statistical mechanics, it is the tube model that seems to be the most empirically useful and successful. In this model, the importance of topological constraints or entanglement along the contour of strain is carefully considered.[21,22]

In the present article, silica was modified with two different SCAs. The condensation reaction that took place between silica and SCAs was proved by Fourier transform infrared spectroscopy (FTIR). Curing curves were applied to study the cure kinetics of the solution-polymerized styrene-butadiene rubber (SSBR) reinforced by the modified silica (M-Silica). We explored the tensile property and network structure of the filled SSBR by applying tube model theory and nonlinear viscoelastic behaviors, which would lead to a better knowledge of improved properties of the SSBR filled with M-Silica.

EXPERIMENTAL

Materials

Commercial SSBR 2535L (styrene content = 24.8%, vinyl content = 9.70%, $M_w = 16.7 \times 10^4$, PDI = 2.12) was purchased from Gaoqiao Petrochemical Co. Sinopec, (Shanghai, PRC). The precipitated silica (Zeosil 115GR) with specific surface area of 115 m^2/g and pH of 6.5 was kindly provided by Rhodia, Qingdao, P.R.C. SCA bis-(triethoxysilylpropyl)-tetrasulfide (TESPT) and bis-(triethoxysilylpropyl)-bisulfide (TESPD) was products of Nanjing Shuguang Chemical Group Co., PRC.

Surface modification of silica nanoparticles

According to the modification method in the literatures,[13,23] 100 g silica nanoparticles were dispersed in 500 mL ethanol in a flask with stirring for 1 h. Ten grams of SCA (the mass of SCA accounts for 10% of the mass of silica particles) and 0.2 g dibutyltin dilaurate was dissolved in 100 mL ethanol and then poured into the silica-ethanol solution with vigorous stirring for 2 h at 60°C. Dibutyltin dilaurate was used as a catalyst of the condensation reaction between the alkoxy groups of SCA and silanol groups of silica. Finally, the two kinds of coupling agent of M-Silica, TESPT-Silica and TESPD-Silica, were dried under vacuum.

TABLE I
Formulations of the SSBR/Silica Nanocomposites

Ingredients	Amount (phr[a])
SSBR	100
Stearic acid	1
ZnO	2.5
Antioxidant 4020[b]	2
Accelerator CBS[c]	1.7
Accelerator DPG[d]	1.25
Sulfur	1.4
Silica 115GR	50
SCA	10
Curing time (min)	45

[a] Parts by weight per hundred parts of rubber.
[b] *N*-(1,3-dimethylbutyl)-*N*′-phenyl-*p*-phenylenedianine.
[c] *N*-Cyclohexyl-2-benzothiazole sulfonamide.
[d] Diphenyl guanidine.

Preparation of M-Silica/SSBR nanocomposites

The formulation for preparation of varying rubber composites is shown in Table I. All of the ingredients were mixed on a two-roll mill at room temperature. For comparison, two counterparts of the SSBR/M-Silica nanocomposites were obtained by directly adding SCA during compounding, which were denoted as SSBR/Silica/TESPT and SSBR/Silica/TESPD, respectively. The cure time was determined using an oscillating disc rheometer (ODR) at 150°C.

Measurements and characterization

FTIR analysis of M-Silica was carried out on a TENSOR 27 FTIR spectrometer (BRUKER, German). The samples were pressed into pellets with KBr. The spectral range is 400–4000 cm^{-1}. A resolution of 4 cm^{-1} was chosen. It is noted that all the M-Silica samples were extracted by ethanol for 48 h to remove the ungrafted SCAs and then dried in vacuum at 40°C for 12 h.

The tensile strength was tested with an SHIMADZU, AG-20KNG material testing machine (with a 1 kN load cell) at room temperature with tensile rate of 500 mm min^{-1} according to the GB/T1040-92 standard. The initial length and thickness of samples were 25 mm and 2 mm. For each test, five parallel measurements were carried out and the average value was taken.

Bound rubber content was determined by extracting the unbound materials, such as nonrubber ingredients and free rubbers, with toluene for 7 days at room temperature and drying for 2 days at room temperature. Masses of the samples before and after

extraction were measured and the bound rubber content was calculated as follows:

$$R_b(\%) = 100 \times \frac{W_{fg} - W_t[m_f/(m_f + m_r)]}{W_t[m_f/(m_f + m_r)]} \quad (1)$$

where R_b is the bound rubber content, W_{fg} the mass of filler and gel, W_t the mass of the sample, m_f the mass fraction of the filler in the compound, and m_r the mass fraction of the rubber in the compound.

Crosslink density (υ) was determined by equilibrium swelling measurements on the basis of the Flory–Rhener equation[24]:

$$-[\ln(1-\Phi_r) + \Phi_r + \chi\Phi_r^2] = V_0 n\left[\Phi^{1/3} - \frac{\Phi_r}{2}\right] \quad (2)$$

where Φ_r is the volume fraction of polymer in the swollen mass, V_0 is the molar volume of the solvent (106.2 cm^3 for toluene), n is the number of active network chain segments per unit volume (crosslinking density), χ is the Flory–Huggins polymer–solvent interaction term. The value of χ for toluene-rubber is 0.44.[25] The value of Φ_r was reached according to the method used by Bala et al.,[26]

$$\Phi_r = \frac{w_2/\rho_2}{w_2/\rho_2 + (w_1 - w_2)/\rho_1} \quad (3)$$

where w_1 and w_2 are the weights of the swollen and deswollen samples, respectively, and ρ_1 and ρ_2 are the densities of the solvent and the polymer.

Viscoelastic properties of the samples were measured on a TA 2980 (TA Instrument, New Castle (Delaware), USA) analyzer. The samples were trimmed to the following dimensions: 10 mm in length, 5 mm in width, and 1.0 mm in thickness. The properties were measured by using tension clamp in the temperature range from −100 to 100°C at a heating rate of 3 K/min. The tests were carried out at a frequency of 2 Hz. The Payne effect was measured at room temperature in the dynamic amplitude range of 0–5000 μm. The tests were carried out at a frequency of 1 Hz.

The micromorphologies of the samples were examined with transmission electron microscopy (TEM). Ultrathin sections of the specimens were prepared at −100°C using a Leica Ultracut-R ultramicrotome. The thin slices were put on copper grids and then submitted to TEM observation with a JEOL JEM 2010 TEM under an accelerating voltage of 200 kV.

RESULTS AND DISCUSSION

Structure characterization of M-Silica by FTIR

The modification of silica surface is achieved by reaction of hydroxyl groups from silica with silanol groups formed by hydrolysis of the SCAs. Therefore, the grafting reaction can be easily identified by the appearance of characteristic bands of TESPT and TESPD in M-Silica FTIR spectra, such as —CH_2— appearing at 2920–2950 cm^{-1}. Figure 1 shows FTIR spectra of unmodified silica, M-Silica, and SCAs ((a) for a TESPT and (b) for TESPD). It can be seen that the peak of —CH_2— exists in TESPT and TESPD modified silica, which is the evidence that SCA molecules are grafted on the silica surface.

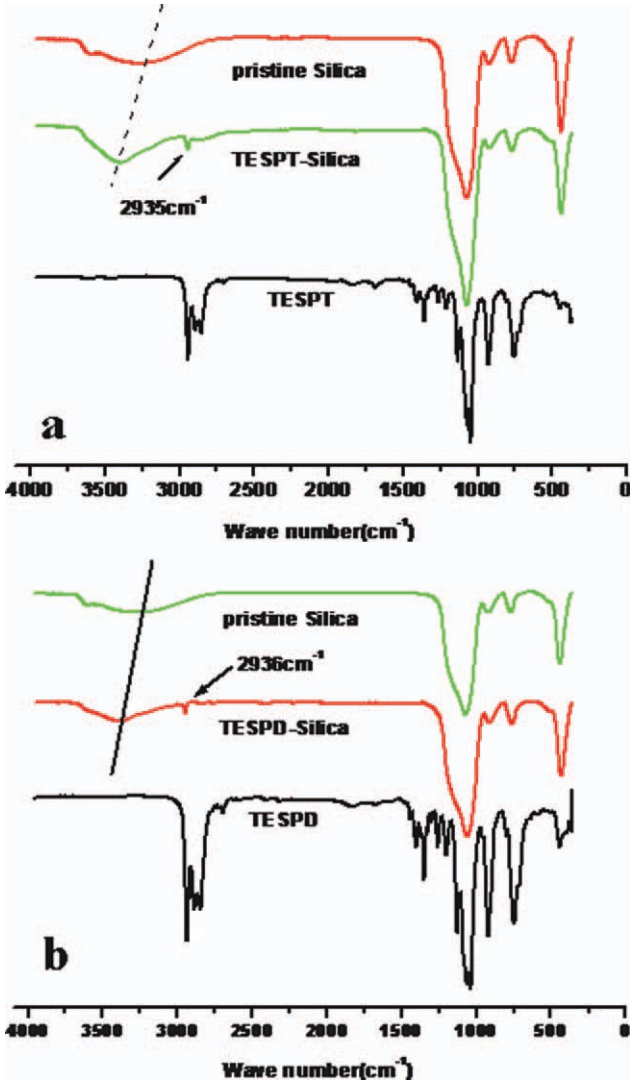

Figure 1 FTIR spectra of unmodified silica and silica modified by SCAs: (a) TESPT; (b) TESPD. [Color figure can be viewed in the online issue, which is available at wileyonlinelibrary.com.]

To further confirm the graft reaction, we examined the —OH vibration on the silica surface before and after grafting. By comparing the position of Si—OH peaks, it can be found that the Si—OH band at 3600–3000 cm^{-1} in the M-Silica shifted toward the direction of higher wave numbers, which is called "blue shift." The reason for the "blue shift" of hydroxyl groups can be considered as destruction of hydrogen

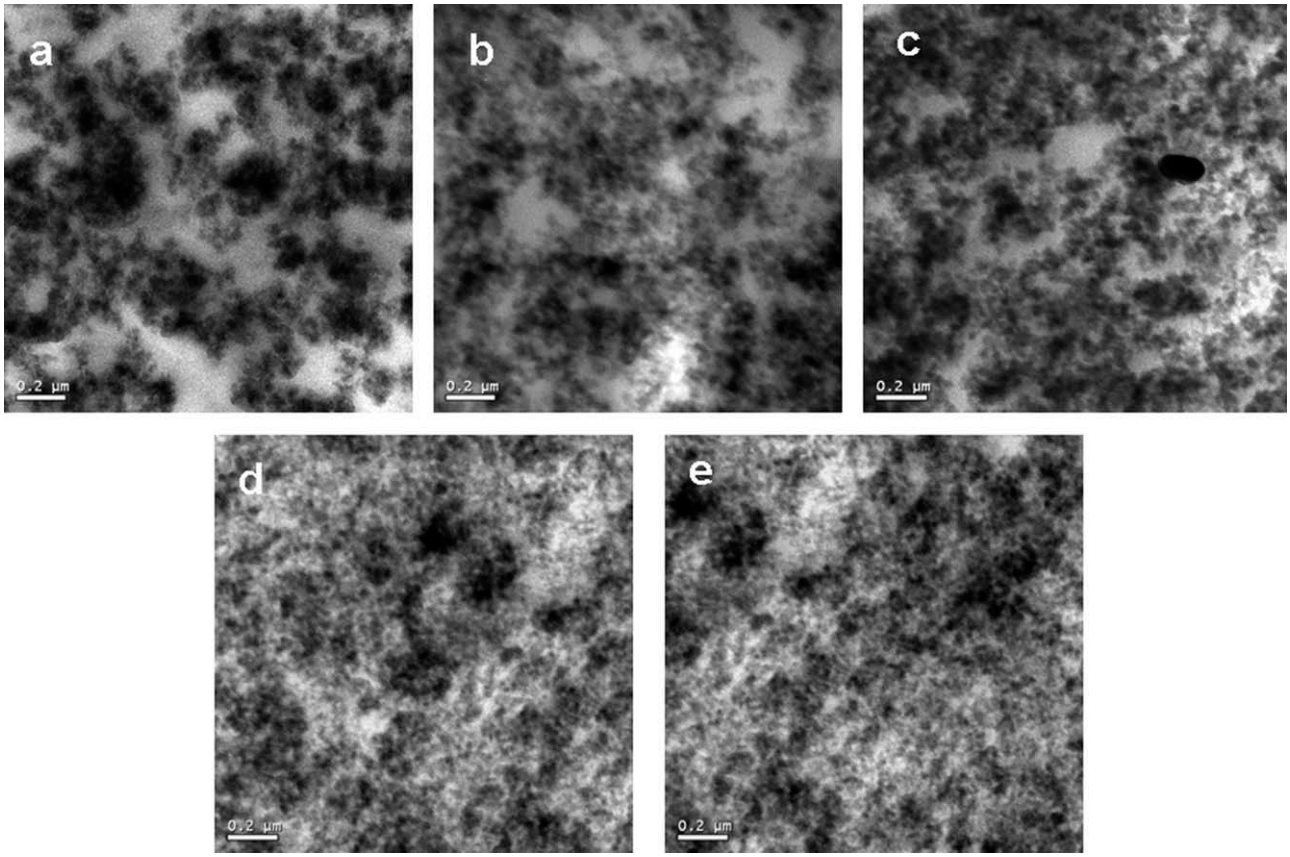

Figure 2 TEM photos of SSBR/silica nanocomposites: (a) SSBR/silica; (b) SSBR/silica/TESPT; (c) SSBR/silica/TESPD; (d) SSBR/TESPT-silica; (e) SSBR/TESPD-silica.

bonds existing at the surface of silica. The poor dispersity of silica is due to the fact that the hydroxyl groups on the filler surface can form hydrogen bonds resulting in easy aggregation of silica particles. Hence, the destruction of hydrogen bond favors the dispersion of silica particles in rubber matrix.

Morphology observation

Generally speaking, the dispersion state of the fillers in the rubber matrix is one of the decisive factors in determining the ultimate properties of the filled-rubber composites. Homogeneous dispersion of the filler especially in nanoscales leads to enhanced properties of the resulting composites. On the contrary, the aggregated fillers in the rubber matrix act as the stress-concentration points, leading to deterioration of macroscopic properties. Figure 2 demonstrates the state of dispersion of unmodified and modified silica in the SSBR matrix. It can be seen from TEM images that large silica particles embed in the unmodified silica-filled SSBR, which results in poor filler–rubber interactions. As adding directly SCA in the filled SSBR, the dispersion of the filler is improved to some extent. The modified silica presents relatively uniform and homogeneous dispersion in SSBR matrix and silica particles have a relatively narrow distribution.

Cure kinetics

In order to reveal the structure and properties of the SSBR/M-Silica composites, it is needed to study the cure kinetics further. The kinetics of the cure reaction can be related to time and temperature using a mathematical equation. Generally speaking, chemical reaction can be divided into single reaction and autocatalytic reaction.

In a single reaction, the basic rate equation is given as[27]:

$$\frac{d\alpha}{dt} = K(T)(1-\alpha)^n \tag{4}$$

where $d\alpha/dt$ is the cure rate, t is the time, n is the order of reaction, and $K(T)$ is the temperature-dependent reaction rate constant.

In an autocatalytic reaction, the equation is given as[28]:

$$\frac{d\alpha}{dt} = K(T)\alpha^m(1-\alpha)^n \tag{5}$$

where m is the order of the reaction.

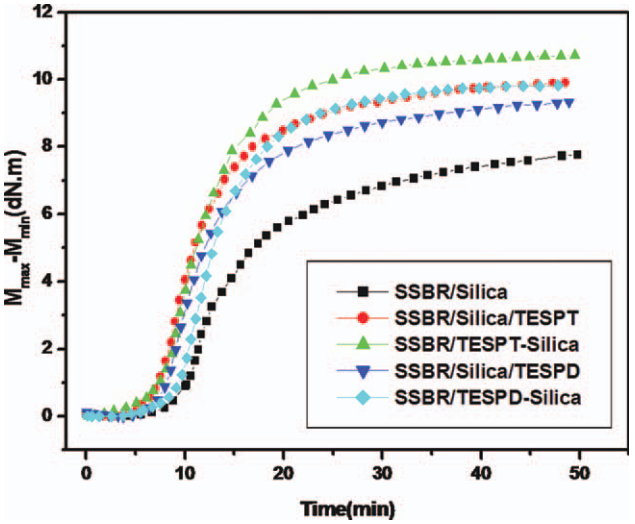

Figure 3 M_{max}–M_{min} vs. time for SSBR filled with modified and nonmodified silica. [Color figure can be viewed in the online issue, which is available at wileyonlinelibrary.com.]

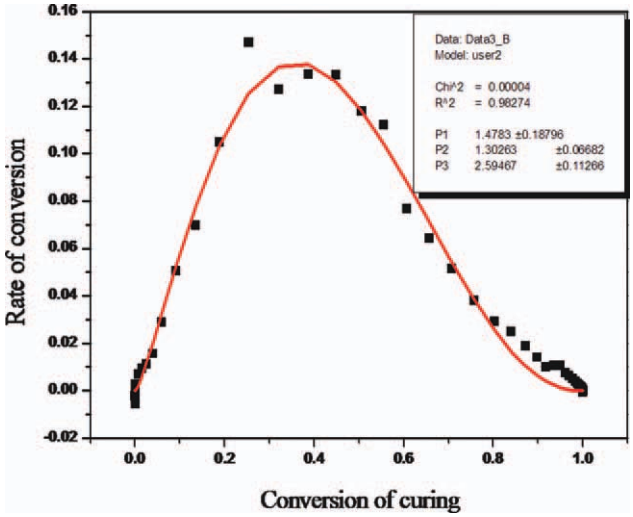

Figure 4 Rate of conversion as a function of conversion of the SSBR/TESPT-silica. Solid line represents theoretical curve and square dots represent experiment data. [Color figure can be viewed in the online issue, which is available at wileyonlinelibrary.com.]

A kinetics model should be first chosen in order to decide which equation should be adopted. In a simple reaction, the maximum rate of curing occurs at the beginning, whereas in an autocatalytic reaction, the maximum rate of curing occurs at a conversion degree other than zero because it is promoted by the products of the reaction.[29] According to our experiments, the curing of the filled-SSBR samples fit the autocatalytic reaction model. So eq. (5) was used to reveal the cure kinetics of filled SSBR.

When the curemeter is used to study the cure kinetics, α is defined as follows[30]:

$$\alpha = \frac{M_t - M_0}{M_{max} - M_0} \tag{6}$$

where M_0, M_t, and M_{max} are the torque values at time zero, at curing time t, and at the end of the cure process.

Figure 3 shows the curing curves. As M-Silica was introduced into the rubber systems, the $M_{max} - M_{min}$ value increases, which is related to the crosslink density.[31] This means that the addition of M-Silica increases the crosslink efficiency and crosslink density of the SSBR composites compared with the incorporation of pristine silica. Then eq. (5) was used to determine the kinetic parameters (n, m, and K) of vulcanization. Figure 4 manifests the rate of conversion ($d\alpha/dt$) as a function of the conversion (α) of SSBR filled with TESPT-Silica. The kinetic parameters can be obtained by linear multiple regression analysis of the experimental data using ORIGIN 7.0 computer software. Similarly, the kinetic parameters of the SSBR filled with different kinds of silica can be also attained. The results are listed in Table II. When rubber is filled with M-Silica, the kinetic parameters change. The values of K of the filled rubbers are larger than the corresponding value of the SSBR/Silica, suggesting that M-Silica affects and accelerates the curing reaction. The values of n, m of the filled SSBR also increase compared with SSBR/Silica, indicating that the reaction order changes, that is, SCA has taken part in the curing reaction of SSBR. As we know, TESPT and TESPD involve four and two sulfur atoms in one molecule, respectively, which can react with diene unit of SSBR.[32] In order to gain deeper information, the kinetic parameters of the SSBR/Silica/SCAs were calculated for comparison with those of the SSBR/M-Silica. As listed in Table II, it is apparent that curing kinetics of the M-Silica/SSBR differs from that of Silica/SCA/SSBR. This fact leads to an inference that the dispersion of SCA in the rubber matrix plays an important role in curing process of the SSBR systems. As SCA molecules were grafted onto

TABLE II
Kinetic Parameters of the Curing Obtained from Curemeter Testing

	K^a (150°C)	n^b	m^c
SSBR/Silica	0.83086	2.12517	0.91323
SSBR/TESPT-Silica	1.47830	2.59467	1.30263
SSBR/TESPD-Silica	1.31687	2.36438	1.15496
SSBR/Silica/TESPT	1.24701	2.65206	1.21215
SSBR/Silica/TESPD	1.16984	2.43347	0.99425

[a] $K(T)$ is the temperature-dependent reaction rate constant.
[b] n is the order of the reaction.
[c] m is the order of the reaction

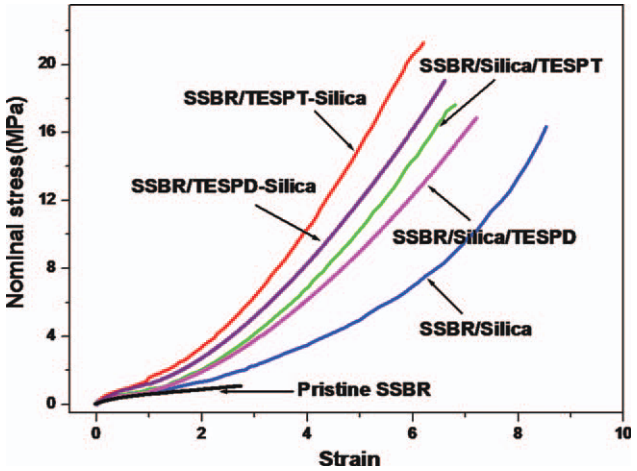

Figure 5 Stress–strain curves for filled SSBR. [Color figure can be viewed in the online issue, which is available at wileyonlinelibrary.com.]

the silica particles, molecular barriers form between the filler particles and the rubber matrix, which probably results in less restriction on the rubber molecular chains exerted by fillers. The role the SCA molecules grafted on the silica surface play can be regarded as a quasi-plasticizer which leads to an enhanced mobility of rubber chain adsorbed onto filler surface and then accelerates the crosslink reaction.

Stress–strain behaviors

The stress–strain curves of pristine and the filled SSBR were displayed in Figure 5, Effective enhancement in tensile property can be achieved by introducing silica into SSBR as indicated in Figure 5. The stress at break is increased by 13.4 times from 1.13 MPa for pristine SSBR to 16.3 MPa for the filled SSBR with 50 wt % silica. SSBR filled with M-Silica exhibits further improvement in tensile strength which goes up from 16.3 MPa for SSBR/Silica to 21.3 MPa. It is worth noting that improvement in stress of the M-Silica is obviously superior to that of silica and SCA separately added during the compounding process as aforementioned.

It is well known that the stress–strain curves for the silica-filled rubber system are affected by the crosslink density of the rubber matrix,[33] the size of agglomerates formed by silica,[34,35] and rubber/silica interactions.[36] The crosslink densities of different silica-filled SSBR samples are shown in Table III. The comparison of the data reveals that the M-Silica-filled SSBRs exhibit higher values than the SSBR/Silica/SCA samples. As a matter of fact, the crosslink density from the equilibrium swelling measurement involves two parts, namely chemical crosslink density derived from the vulcanization reaction and physical crosslink density attributed to the filler–rubber interactions. According to the study of cure kinetics, dispersion of SCA in the rubber matrix may affect the barriers of crosslink reaction, leading to the difference in chemical crosslink density. On the other hand, when the SCA is grafted on silica particles, a hydrophilic character of the particle changed into a hydrophobic one, which enhances the filler–rubber interaction and then increases the physical crosslink densities.[5]

It is not surprising that the most important properties of rubbers depend on the network structure. A wealth of experimental evidence has clearly demonstrated that the stress–strain behavior is controlled not only by crosslink density, but also by the contributions from the uncrossability of the network chains (constraint contributions).[37–39] Therefore, in order to reach better understanding of the reinforcement mechanism and the influence of silica modified by SCA on the SSBR network structure, the contribution of crosslink and constraint contributions to the stress–strain behaviors should be separated by applying the tube model theory. In this theory, the mechanical properties of the filled elastomers depend strongly on the number of elastically effective polymer–polymer crosslinks, the lateral tube dimension in the mobile polymer phase, and the elastically effective number of polymer–filler junctions.[40,41] The following uniaxial stress–strain relation consists of two contributions:

$$\sigma_M = \frac{\sigma}{(\lambda - \lambda^{-2})} = G_c + G_e f(\lambda) \tag{7}$$

σ_M is the reduced stress, G_c is the elastic modulus that is relative to the contributions of effective crosslink density, G_e corresponds to the topological tube-like constraints, and $f(\lambda)$ is the deformation function which is given by the following equation:

$$f(\lambda) = \frac{2}{\beta}\frac{\lambda^{\beta/2} - \lambda^{-\beta}}{\lambda^2 - \lambda^{-1}}, \quad f(\lambda = 1) = 1, \tag{8}$$

where β can be considered as an empirical parameter which describes the relation between the deformation tube in the stretched state and an undeformed tube corresponding to the equilibrium state. In general, β is taken as 1.

TABLE III
Crosslink Densities for Different Silica Filled SSBR Composites

Sample code	Crosslink density ($\times 10^{-3}$mol cm^{-3})
SSBR/Silica	1.21
SSBR/TESPT-Silica	2.29
SSBR/TESPD-Silica	2.03
SSBR/Silica/TESPT	2.05
SSBR/Silica/TESPD	1.81

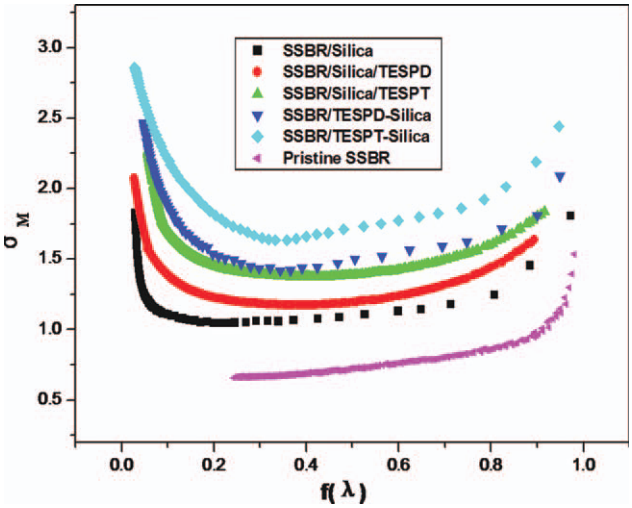

Figure 6 Mooney-stress vs. deformation function f of the tube-like contribution to the tensile strength. [Color figure can be viewed in the online issue, which is available at wileyonlinelibrary.com.]

Because of the existence of filler particles, the effective strain ratio of the rubber portion is larger than the macroscopic one. In the simplest model, no deformation of the filler particles and uniform deformation of the rubber portion are assumed. Therefore, the deformation λ must be replaced by the real deformation ratio λ′, which is expressed as:

$$\lambda' = (\lambda - 1)\chi_{\text{eff}} + 1 \tag{9}$$

where the effective amplification factor, χ_{eff}, is given by the following expression:

$$\chi_{\text{eff}} = 1 + 2.5f\Phi_{\text{eff}} + 14.1\Phi_{\text{eff}}^2 = \frac{G}{G_0} \tag{10}$$

Based on eqs. (7)–(10), the Mooney σ_M vs. deformation was plotted, as shown in Figure 6. The moduli G_c and G_e were determined from the linear part of intermediate deformation in the curves. It is obvious that as the network chain is stretched, the reduced stress goes down at moderate deformation. This can be ascribed to the occurrence of entanglement slippage. At higher deformation, a large and abrupt upturn can be observed for all the samples which are frequently attributed in the literatures to the limiting polymer chain extensibility and also to strain-induced crystallization. SBR is noncrystallizable rubber as described in the literatures. So the steep increase in the stress–strain is due to limitation of polymer chain extensibility.[42,43]

In the tube model theory, some network parameters can be estimated from G_c and G_e. G_c is relative to the average molecular mass between network chains, M_c, as presented in eq. (11). Constraint modulus, G_e, is associated with the lateral dimensions of the configurational tube with the bulk rubber by eq. (12).[44]

$$G_c = \rho_P RT/M_c \tag{11}$$

$$G_e = \frac{1}{4 \times (6)^{1/2}} K_B T n_s \left(\frac{l_s}{d_0}\right)^2 \tag{12}$$

where ρ_P is polymer density, R is the gas constant, and K_B is the Boltzmann constant. l_s is the average length of the Kuhn's statistical segment (1.06 nm is taken for SBR[45]). n_s, the polymer segment number density, can be taken as 3.85 nm^{-3} from the literature.[46] d_0 is the lateral tube dimension, which is equal to the mean spacing between two successive entanglements in the mobile rubber phase.

The typical network parameters calculated from eqs. (11) and (12) are listed in Table IV. Compared with pristine SSBR, SSBR filled with unmodified silica presents major differences in both values of G_c and G_e. These phenomena can be described through the entanglement-bound rubber model (EBRM).[47] According to EBRM, the silica affects the rubber property through the filler–rubber interaction, which is controlled by the entangled bulk rubber with bound rubber in a transition zone between the highly immobilized and localized bound rubber and the mobile bulk rubber phases. Because a single molecule of bound rubber is likely to adsorb on silica surface site, the bound rubber is essentially immobile in this model. The strong transition zone layer produces an increase of G_c, because of the formation of strong filler–rubber interaction. The entanglement slippage is reduced due to bound rubber around silica particles, which is reflected in the decrease of G_e. In spite of the reduction of the contribution of topological constraints, total contribution of G_c and G_e is increased in the presence of silica particles. For this reason, the tensile strength of Silica/SSBR is larger in comparison to that of pristine SSBR.

Surprisingly, the M-Silica-filled SSBR network exhibits increase in both G_c and G_e values. Apparently, the larger value of G_c stems from the increase of crosslinks due to the additional reactions of sulfur atoms in SCA with SSBR and enhanced interaction

TABLE IV
Typical Parameters of Different Samples Networks

Sample code	G_c	G_e	M_c	d_0 (nm)
SSBR	0.452	0.386	2661	2.15
SSBR/Silica	0.810	0.259	1655	2.63
SSBR/TESPT-Silica	1.352	0.441	997	2.01
SSBR/TESPD-Silica	1.206	0.435	1081	2.03
SSBR/Silica/TESPT	1.184	0.401	1132	2.11
SSBR/Silica/TESPD	1.083	0.392	1316	2.13

TABLE V
Bound Rubber Content of Filled SSBR Composites

Sample code	Bound rubber content (%)	
	From experimental data	From tube model
SSBR/Silica	34.7	32.0
SSBR/TESPT-Silica	24.3	21.4
SSBR/TESPD-Silica	25.6	22.2
SSBR/Silica/TESPT	28.0	26.1
SSBR/Silica/TESPD	29.1	27.5

between filler and rubber matrix as discussed above. An increase of G_e leads therefore to a reduction in tube diameter d_0, i.e., an enhancement of the configurational constraints, suggesting that the rubber seems to be confined to form a more entangled structure. Such structure is probably responsible for the high performance of the SSBR/M-Silica composites. For SSBR/Silica/SCA, G_e does not change in a significant way in relation to SSBR/Silica.

In order to uncover the reason for the increase of G_e, the bound rubber contents of all the samples in the study were calculated and listed in Table V. It can be observed that when the SCA molecules were grafted on silica particles, the bound rubber content decreases. The similar phenomenon is previously observed in other SSBR filled with SCA-modified silica composites reported by Ramier et al.[48] The difference between Ramier et al.'s and our systems is that the SCA used in our study belonged to sulfur-donor SCA but Ramier et al.'s did not. Sulfur-donor can bring about the formation of covalent bonds between silica and rubber matrix; such covalent bonds can not appear without using it. The amount of bound rubber of the filled SSBR also can be calculated according to the EBRM. The number of units absorbed in the immobilized bound rubber layer on the silica surface is denoted by N_{br} and its relative amount is given by:

$$\frac{N_{\mathrm{br}}}{N_s} = 1 - \left(\frac{G_e(\varphi \neq 0)}{G_e(\varphi = 0)}\right)^{1/2}(1 - \varphi)$$

Here, N_s is the total number of chain units (statistical segments) in the network. Table V yields calculated contents of the polymer absorbed in the immobilized bound rubber layer, which are in agreement with our experimental data. Less amount of bound rubber in the M-Silica-filled SSBR induces a more entangled structure in which the mobility of rubber chain is hindered for lateral fluctuations by the presence of the neighboring chains. Unlike the bound rubber which is totally immobilized, covalent bonds between M-Silica and rubber matrix can rotate freely, so in the particular interface the interaction with rubber matrix is probably weaker than in pristine silica compounds. Distinguished from SSBR/Silica, although SSBR/M-Silica contains less bound rubber, more entanglements are present in the bulk rubber phases, which compensate for the reduced content of bound rubber. Less but sufficient content of bound rubber and more entanglements in the bulk rubber give birth to more homogenous rubber

TABLE VI
Magnitude of the Payne Effect for Filled SSBR

Sample code	E_0' (MPa)	E_∞' (MPa)	$E_0' - E_\infty'$ (MPa)
SBR/Silica	5.60	1.24	4.36
SBR/TESPT-Silica	4.54	1.66	2.88
SBR/TESPD-Silica	4.19	1.51	2.68
SBR/Silica/TESPT	5.17	1.59	3.58
SBR/Silica/TESPD	4.99	1.43	3.56

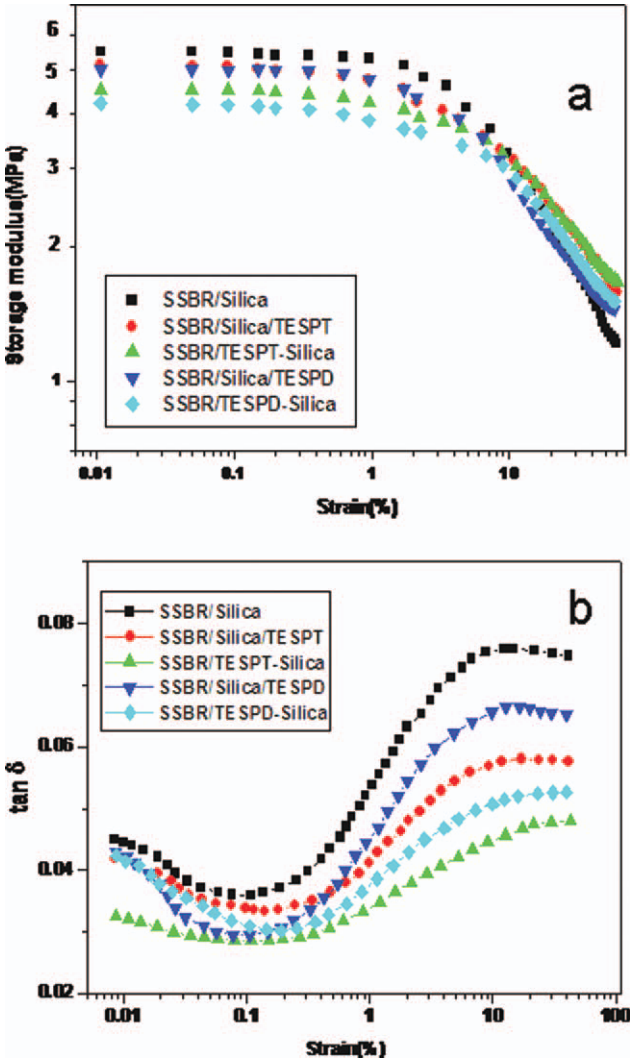

Figure 7 (a) Storage modulus vs. dynamic strain amplitude for silica-filled SBR. (b) tan δ vs. dynamic strain amplitude for the silica-filled SBR. [Color figure can be viewed in the online issue, which is available at wileyonlinelibrary.com.]

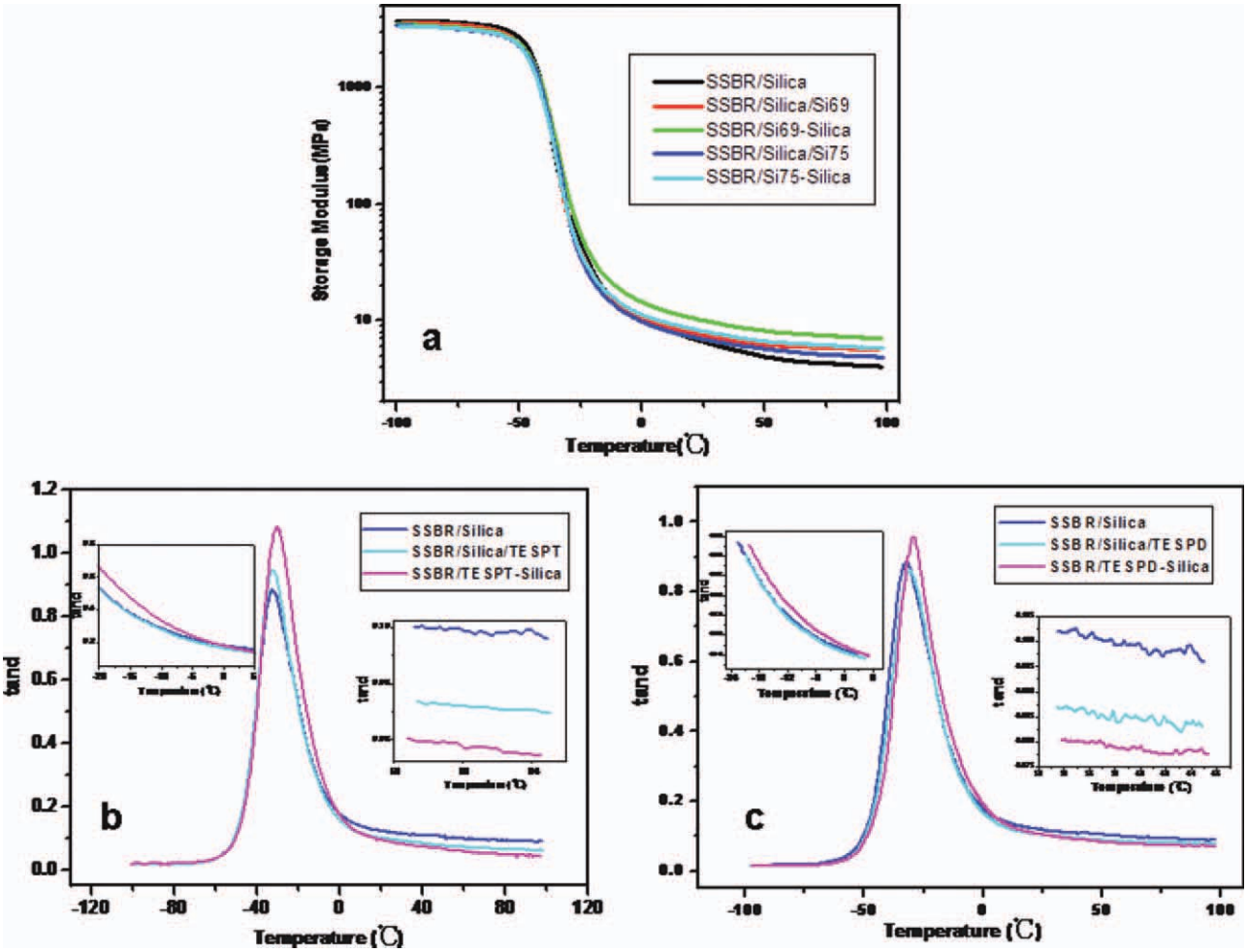

Figure 8 (a) Storage modulus vs. temperature for the filled SSBR. (b) Loss factor vs. temperature for the filled SSBR containing TESPT. (c) Loss factor vs. temperature for the filled SSBR containing TESPD. The inserted figures in (b) and (c) are magnified curves at the temperature adjacent to 0°C and 60°C, respectively. [Color figure can be viewed in the online issue, which is available at wileyonlinelibrary.com.]

network, which favors a higher tensile strength. On the other hand, the number of silica aggregates went down after surface modification of pristine silica, indicating that specific surface area of silica enlarged and accordingly M-Silica could cover a larger rubber percentage than pristine silica. For the whole network, due to the homogeneous dispersion the impact of M-Silica on the rubber molecules is relatively wide, and thus rubber is confined forming a highly ordered and entangled structure.

Viscoelastic behaviors

The nonlinear viscoelastic behavior as a function of strain was investigated. A large reduction in the storage modulus at high strain, associated with the Payne effect, is shown in Figure 7. The storage modulus was the highest ($E_0^{'}$) at small strain amplitude and then decreased monotonically to a low value ($E_\infty^{'}$). The magnitude of Payne effect was measured in terms of the value of $E_0^{'} - E_\infty^{'}$. The modulus plateau was not reached at high dynamic strain amplitude due to the strain limitation of device. As shown in Figure 7 and Table IV, the SSBR reinforced by unmodified silica had a larger magnitude of the Payne effect, indicating more powerful filler–filler interactions and accordingly poor filler–rubber interactions.[49,50] However, when the M-Silica was filled in SSBR, the magnitude of the Payne effect was decreased in that the graft of SCA molecules onto the filler surface minimized the silica–silica interaction. As can been observed in Figure 7(b), the loss factor (tan δ) shows a typical loss peak, which takes place at the approximately the same dynamic amplitude range where the storage modulus is mostly rapidly decreasing.

The dynamic mechanical spectra with temperature of the filled SSBR given in Figure 8 are very enlightening. From Figure 8(a), it can be observed that the SSBR filled with unmodified silica shows largest modulus below the glass transition temperature, whereas the modulus drops fastest compared with

that of the SSBR/M-Silica and SSBR/Silica/SCA in the higher temperature zone(20–70°C). Actually, the strain of samples in the dynamic mechanical analysis with temperature is less than 10%, so according to Figure 7 the dynamic behavior within this strain belongs to linear behavior. In the low temperature domain, the segmental motion was frozen and the filler–filler interaction mainly contributes to the storage modulus. On the contrary, as the temperature goes up to ambient temperature and above, the Payne effect becomes weaker and weaker.[51] At that time, the rubber–filler interaction and rubber network dominate the storage modulus. This could course the fact that the SSBR filled with M-Silica exhibits higher modulus than the SSBR/silica and SSBR/silica/SCA in higher temperature.

It can be observed from Figure 8(b,c) that a notable increment in intensity of tan δ at glass transition temperature was observed in the M-silica-filled SSBR. This phenomenon has the same origin with the fact that the SSBR/silica shows largest modulus below the glass transition temperature. Better dispersion of the M-silica reduced the formation of secondary filler network, which decreased the amount of rubber trapped within the secondary filler network.[7] This means more rubber molecules can involve in the segment relaxation. On the other hand, what should be noted is that in the high temperature region between 20°C and 70°C, tan δ of the SSBR/M-silica presents the lowest value which facilitates a good rolling resistance. The enhancement of rubber network and entangled structure provoked higher elasticity of the SSBR filled with M-silica, which is the main reason for lowest tan δ value.

CONCLUSIONS

In the present article, the modification of silica was carried out by condensation reaction between hydroxyl groups on the silica surface and silanol groups formed by hydrolysis of the SCAs, which was confirmed by the FTIR spectra. Compared with the pristine silica-filled SSBR, the SSBR reinforced by the M-Silica presents not only better filler dispersity and mechanical properties but also lower internal friction in the certain temperature range. The kinetics parameters of the SSBR/M-Silica varied from those of SSBR with pristine silica due to the fact that SCA molecules grafted on the silica surface provoked an enhanced mobility of rubber chain adsorbed onto filler surface and then decreased the barrier of crosslink reaction. This was also proved by the variation of bound rubber content. Tube model theory was used to analyze the mechanism of reinforcement in tensile strength achieved by the M-Silica. SSBR containing the M-Silica exhibited a combination of increments in topological tube-like constraints and crosslink density in comparison with the SSBR filled with pristine silica. Strain dependence of dynamic modulus revealed that the secondary network formed by the silica particles was destroyed to some extent with the increase of the hydrophobic character of silica surface. The loss factor of the SSBR/M-Silica was dominated by different mechanism in different temperature range, i.e., secondary filler network at glass transition temperature and rubber network and entangled structure above room temperature. The lower tan δ at 60°C facilitates a good rolling resistance.

References

1. Rauline, R. U.S. Pat. US005,227,425A (1993).
2. Heinrich, G.; Dresden, T. A.; Mainz, V. Kautschuk Gummi Kunststoffe 2008, 61, 368.
3. Ou, Y. C.; Yu, Z. Z.; Vidal, A.; Donnet, J. B. Rubber Chem Technol 1994, 67, 834.
4. Mathew, G.; Huh, M. Y.; Rhee, J. M.; Lee, M. H.; Nan, C. Polym Adv Technol 2004, 15, 400.
5. Suzuki, N.; Ito, M.; Yatsuyanagi, F. Polymer 2005, 46, 193.
6. Choi, S. S.; Kim, I. S.; Woo, C. S. J Appl Polym Sci 2007, 106, 2753.
7. Valentın, J. L.; Posadas, P.; Marcos-Fernandez, A.; Ibarra, L.; Rodrguez, A. J Appl Polym Sci 2006, 99, 3222.
8. Yan, H. X.; Sun, K.; Zhang, Y.; Zhang, Y. X.; Fan, Y. Z. J Appl Polym Sci 2004, 94, 1511.
9. Meledina, L.; Kandyrin, K.; Knee, C. S.; Zaikov, G. Macromol Symp 2007, 247, 147.
10. Taniguchi, Y.; Shirai, K, Saitoh, H.; Yamauchi, T.; Tsubokawa, N. Polymer 2005, 46, 2541.
11. Zhang, K.; Chen, H. T.; Chen, X.; Chen, Z. M.; Cui, Z. C.; Yang, B. Macromol Mater Eng 2003, 288, 380.
12. Hong, R. Y., Fu, H. P.; Zhang, Y. J.; Liu, L.; Wang, J.; Li, H. Z.; Zheng, Y. J Appl Polym Sci 2007, 105, 2176.
13. Bauer, F.; Ernst, H.; Decker, U.; Findeisen, M.; Glasel, H. J.; Langguth, H.; Hartmann, E.; Mehnert, R.; Peuker, C. Macromol Chem Phys 2000, 201, 2654.
14. Payne, A. R. J Appl Sci 1962, 6, 57.
15. Payne, A. R.; Whitaker, R. E. Rubber Chem Technol 1971, 44, 440.
16. Harwood, J. A. C.; Mullins, L.; Payne, R. J Appl Polym Sci 1965, 9, 3011.
17. Queslel, J. P.; Mark, J. E. Adv Polym Sci 1984, 65, 135.
18. Vilgis, T. A. Comprehensive Polymer Science; Pergamon Press: New York, 1989; p 23.
19. Kuhn, W.; Grun, F. Kolloid Z 1942, 101, 248.
20. James, H. M.; Guth, E. J Chem Phys 1943, 11, 455.
21. Henrich, G.; Vilgis, T. A. Macromolecules 1993, 26, 1109.
22. Heinrich, G.; Straube, E.; Helmis, G. Adv Polym Sci 1988, 85, 33.
23. Liu, X.; Zhao, S. H. J Appl Polym Sci 2008, 108, 3038.
24. Flory, P. J. Principles of Polymer Chemistry; Cornell University Press: Ithaca, NY, 1953; p 576.
25. He, M. J.; Zhang, H. D.; Chen, W. X.; Dong, X. X.; Polymer Physics, 3rd ed.; Fudan University Press: Shanghai PRC, 2007; p 51.
26. Bala, P.; Samantaray, B. K.; Srivastava, S. K.; Nando, G. B. J Appl Polym Sci 2004, 92, 3583.
27. Armand, J. Y.; Vergnaud, J. Thermochim Acta 1987, 121, 381.
28. Piloyan, G. O.; Ryabchikov, I. D.; Novikova, O. S. Nature 1966, 212, 1229.
29. López-Manchado, M. A.; Arroyo, M.; Herrero, B.; Biagiotti, J. J Appl Polym Sci 2003, 89, 1.
30. Kader, M. A.; Nah, C. Polymer 2004, 45, 2237.

31. Arroyo, M.; López-Manchado, M. A.; Herrero, B. Polymer 2003, 44, 2447.
32. Yatsuyanagi, F.; Suzuki, N.; Ito, M.; Kaidou, H. Polym J 2002, 34, 332.
33. Bueche, F. In Reinforcement of Elastomers; Kraus, G., Ed.; Interscience: New York, 1965; Chapter 1.
34. Suzuki, N.; Yatsuyanagi, F.; Ito, M.; Kaidou, H. J Appl Polym Sci 2002, 86, 1622.
35. Yatsuyanagi, F.; Suzuki, N.; Ito, M.; Kaidou, H. Polymer 2001, 42, 9523.
36. Wagner, M. P. Rubber Chem Technol 1976, 49, 703.
37. Gottlieb, M.; Gaylord, R. J. Polymer 1983, 24, 1644.
38. Matzen, D.; Straube, E. Colloid Polym Sci 1992, 270, l.
39. Vilgis, T. A. In Comprehensive Polymer Science; Eastmond, G. C.; Ledwith, A., Eds.; Pergamon Press: Oxford, 1989; p 57.
40. Marrucci, G. Macromolecules 1981, 14, 434.
41. Edwards, S. F.; Vilgis, T. A. Rep Prog Phys 1988, 51, 243.
42. Furukawa, J.; Onouchi, Y.; Inagaki, S.; Okamoto, H. Polym Bull 1981, 6, 381.
43. Pradhan, S.; Costa, F. R.; Wagenknecht, U.; Jehnichen, D.; Bhowmick, A. K.; Heinrich, G. Eur Polym J 2008, 44, 3122.
44. Heinrich, G.; Vilgis, T. A. Macromolecules 1993, 26, 1109.
45. Heinrich, G. Prog Colloid Polym Sci 1992, 90, 16.
46. López-Manchado, M. A.; Vanentin, J. L.; Carretero, J.; Barroso, F.; Arroyo, M. Eur Polym J 2007, 43, 4143.
47. Funt, J. M. Rubber Chem Technol 1988, 61, 842.
48. Ramier, J.; Chazeau, L.; Gauthier, C.; Guy, L.; Bouchereau, M. N. J Polym Sci Part B: Polym Phys 2006, 44, 143.
49. Zhu, Z. Y.; Thompson, T.; Wang, S. Q.; Von Meerwall, E. D.; Halasa, A. Macromolecules 2005, 38, 8816.
50. Wu, Y. P.; Zhao, W.; Zhang, L. Q. Macromol Mater Eng 2006, 291, 944.
51. Gauthier, C.; Reynauda, E.; Vassoillea, R.; Ladouce-Stelandre, L. Polymer 2004, 45, 2761.